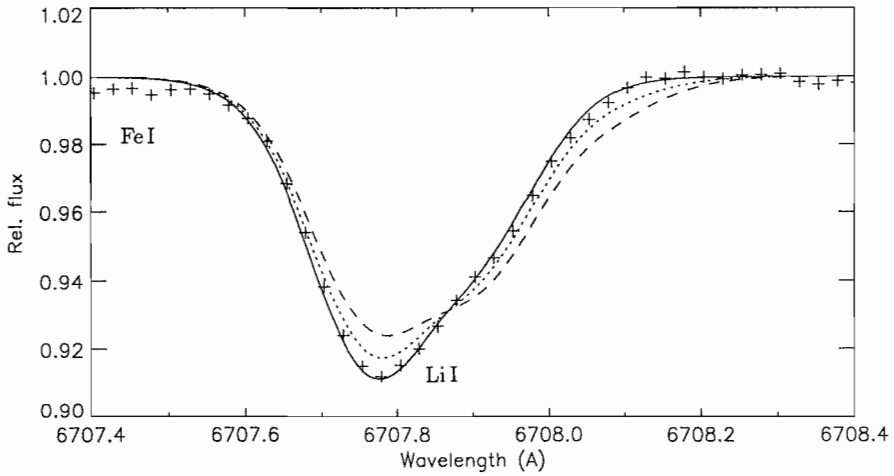

Figure 5: *The observed profile of the Li I line of HD 76932 (+) compared with synthetic model atmosphere profiles convolved with a radial-tangential broadening function with the FWHM = 4.7 km s^{-1} and corresponding to ^{6}Li/Li = 0.0, 0.1 and 0.2, respectively. The position of a weak Fe I line at 6707.4 Å is marked.*

(> 400) and accurate wavelength calibration are to be obtained. A dedicated spectrometer with a well-defined profile similar to the CES but allowing resolutions up to R = 300,000 for a limited spectral region, say $\Delta\lambda = 100$ Å, would be a better instrument for a ^{6}Li programme. In addition, such an instrument would be needed for many other programmes like studies of the hydrodynamics of stellar atmospheres and the composition of interstellar gas.

References

Andersen, J., Gustafsson, B., Lambert, D.L. 1984, *A&A* **136**, 65.

Dravins, D. 1987, *A&A* **172**, 211.

Dravins, D., Lindegren, L., Nordlund, Å. 1981, *A&A* **96**, 345.

Edvardsson, B., Andersen, J., Gustafsson, B., Lambert, D.L., Nissen, P.E., Tomkin, J. 1993, *A&A* **275**, 101.

Edvardsson, B., Gustafsson, B., Johansson, S.G., Kiselman, D., Lambert, D.L., Nissen, P.E., Gilmore, G. 1994, *A&A* (in press).

Gilmore, G., Gustafsson, B., Edvardsson, B., Nissen, P.E. 1992, *Nature* **357**, 379.

Gray, D.F. 1976, "The Observation and Analysis of Stellar Photospheres", John Wiley and Sons, p. 426.

Kurucz, R.L. Peytremann, E. 1975, Smithsonian Astrophys. Obs. Spec. Rep. 362.

Lemoine, M., Ferlet, R., Vidal-Madjar, A., Emerich, C., Bertin, P. 1993, *A&A* **269**, 469.

Maurice, E., Spite, F., Spite, M. 1984, *A&A* **132**, 278.

Meissner, K.W., Mundie, L.G., Stelson, P.H. 1948, *Phys. Rev.* **74**, 932.

Meyer, D.M., Hawkins, I., Wright, E.L. 1993, *ApJ* **409**, L61.

Nave, G., Johansson, S., Learner, R.C.M., Thorne, A.P., Brault, J.W. 1994, ApJS (in press).

Pilachowski, C.A., Hobbs, L.M., De Young, D.S. 1989, *ApJ* **345**, L39.

Smith, V.V., Lambert, D.L., Nissen, P.E. 1993, *ApJ* **408**, 262.

Spite, F., Spite, M. 1982, *A&A* **115**, 357.

The Kinematics of the Planetary Nebulae in the Outer Regions of NGC 1399

M. ARNABOLDI[1], K.C. FREEMAN[1], X. HUI[2], M. CAPACCIOLI[3,4] and H. FORD[5]

[1]*Mt. Stromlo Observatory, Canberra ACT, Australia*

[2]*Astronomy Department, California Institute of Technology, Pasadena, U.S.A.*

[3]*Dipartimento di Astronomia, Università di Padova, Padova, Italy*

[4]*Osservatorio Astronomico di Capodimonte, Napoli, Italy*

[5]*Physics and Astronomy Department, The John Hopkins University, Baltimore, U.S.A.*

1. Introduction

Integrated light observations of the inner regions of giant elliptical galaxies indicate that most of them are slow rotators (e.g. Capaccioli & Longo 1994), with specific angular momentum J/M that is 5 to 10 times less than for the disks of giant spirals (e.g. Fall 1983). Cosmological simulations (e.g. Zurek et al. 1988) show that J/M should be similar in a cluster environment (where spheroidal systems are preferentially found) and in the field (where the disk galaxies predominate). As a way around this problem, Hui et al. (1993) suggested that much of the angular momentum of these elliptical galaxies may reside in their outermost parts (beyond 20 kpc), which cannot be studied by integrated light techniques. This suggestion was made following the recent radial velocity measurements of 500 planetary nebulae (PN) in the giant elliptical Centaurus A, extending out to about 20 kpc from the nucleus (for comparison, kinematical observations from integrated light reach out only about 5 kpc from the nucleus). The velocities of the PNe in Cen A showed a surprising result: its outer halo is rapidly rotating. The mean rotational velocity rises slowly from the centre of the galaxy and flattens to a value of about 100 km/s between 10 and 20 kpc from the centre. This property was not at all apparent from the integrated light observations of the inner regions. Another very interesting dynamical feature of Cen A is that its metal-weak globular cluster system, which also extends out to about 20 kpc, does not appear to be rotating at all (Harris et al. 1988).

Cen A is an unusual and disturbed elliptical system. One would like to investigate the outer halo of undisturbed ellipticals to see (i) if their old stellar populations are also rapidly rotating and (ii) if their globular cluster systems are non-rotating, as in Cen A. It would be interesting to make such a study for normal giant ellipticals and also for the dominant giant ellipticals in clusters. Many of these cD galaxies have huge globular cluster populations and extended halos, and may well have different formation histories. The nearest of these giant galaxies, at distances of

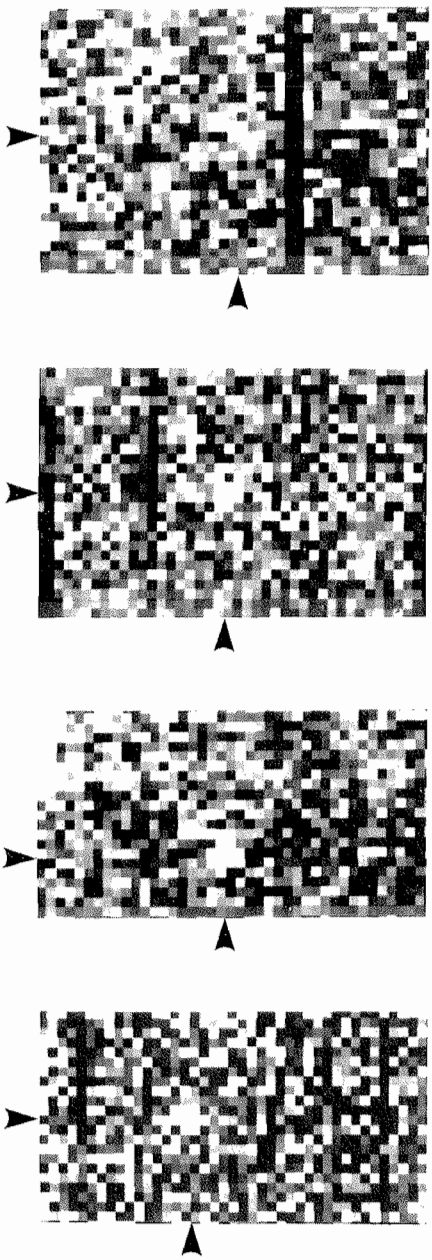

Figure 1: *Images of the 2D spectra of some individual PNe in NGC 1399. In each image, the wavelength direction lies along the long axis, and the spatial direction (i.e. the direction along the slitlet) lies along the short axis. Each image shows about 40 Å in wavelength. The spatial extent of the images varies but can be estimated from the pixel scale of 0.35 arcsec per pixel. The λ5007 Å emission is indicated by the arrows.*

about 15 Mpc, have until now been out of reach for studies of PN kinematics. In this paper we present our new data, from the NTT and EMMI, on the dynamics of the PNe in the outer regions of the cD galaxy NGC 1399 in the Fornax Cluster (adopted distance Δ = 16.9 Mpc). We chose this galaxy as our first candidate, because Grillmair et al. (1994) have already studied the kinematics of its globular cluster system, showing that is has negligible rotation. Our measurements of the PNe kinematics in NGC 1399 extend out to a radius of 4.5 arcmin or 24 kpc, where the blue surface brightness of the integrated light is about 25 mag arcsec^{-2}.

Under subheading 2 we describe the observations and instrumental set-up for these observations. We discuss the data reductions and the errors in our velocity measurements under 3, the results under 4, and the conclusions are drawn under subheading 5.

2. Observations

We acquired spectra for 57 planetary nebulae in NGC 1399 with the ESO NTT at La Silla on November 14–16, 1993. We used the EMMI spectrograph in the red imaging and low dispersion mode (RILD) with multi-object spectra (MOS) plates, the FA 2048 Loral CCD (15 μm ≡ 0.35 arcsec pixels), and the #5 grism: this gives a wavelength range of 4120 to 6330 Å and a dispersion of 1.7 Å per pixel. The only emission line visible in the spectra of these faint PNe is [OIII] λ 5007 Å, so a filter with λ_c = 5050 Å and FWHM = 500 Å was used in front of the grism to reduce the wavelength range of each spectrum. This allowed us to increase the number of slitlets in each MOS mask and also to get enough emission lines from the calibration exposures for an accurate wavelength calibration. The size of the slitlets punched in the MOS plates is 1.2″ × 8.6″. Because the intrinsic width of the [OIII] λ 5007 Å line in PNe is only about 0.5 Å, the detection of faint extragalactic PNe against the sky and galaxy background will be more effective with the higher resolution of the EMMI f/5.3 camera when it becomes available.

Production of the MOS plates – Astrometry and [OIII] photometry for 60 PNe in NGC 1399 came from McMillan et al. (1993). We could not use their precise (α, δ) positions directly to produce the MOS plates, since an accurate map of the distortion in the NTT focal plane (NTT-fp) was not available. McMillan et al. kindly provided us with their deep (4-hour exposure) narrow-band [OIII] image of NGC 1399, acquired at the prime focus imager of the CTIO 4-m telescope with a Tektronix 1024 CCD (8′ × 8′ field and 0.47″ per pixel), from which the PNe were originally discovered. We were able to map the focal plane of the CTIO telescope on to the NTT-fp in a rather lengthy procedure

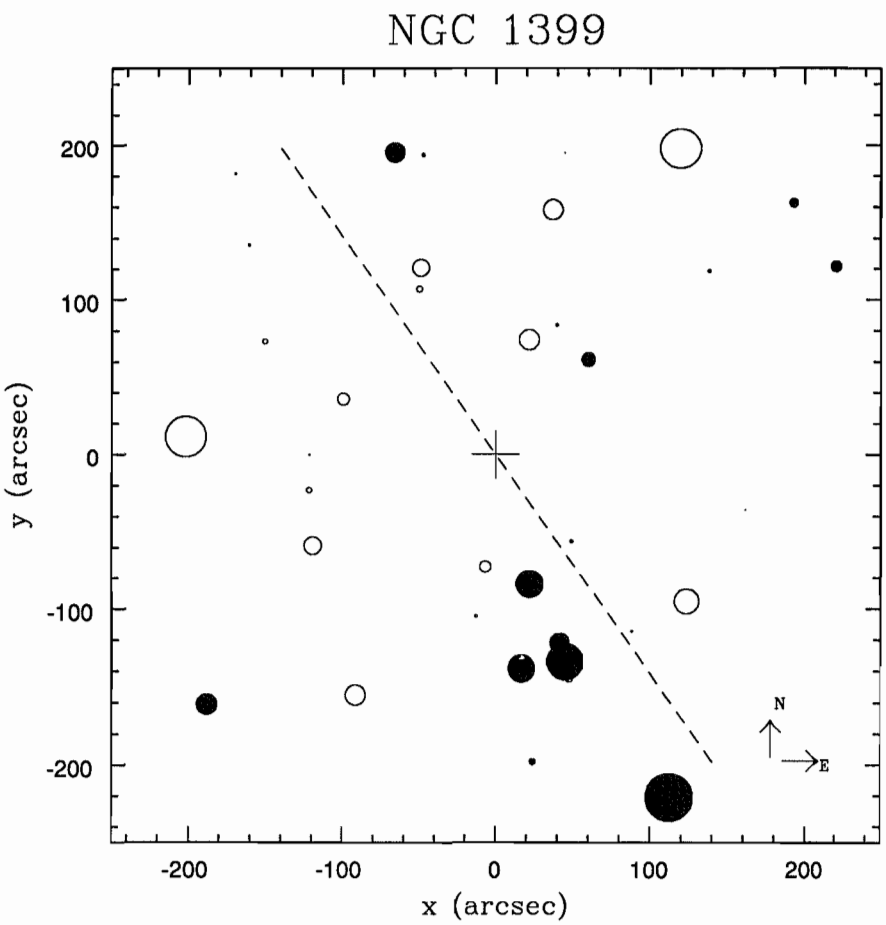

Figure 2: *Positions of the PNe in the NGC 1399 field. The cross corresponds to the galaxy centre, North is up, East on the right. Full dots indicate velocities above the mean value $\bar{v}$ = 1503 km/s, open dots indicate velocities below $\bar{v}$. The size of the circle is proportional to the ratio* $|\ v_{obs}/\bar{v} - 1\ |$. *The dashed line shows the direction of maximum velocity gradient.*

that was essential to the success of the observations.

To make this mapping, we requested a 5-min V-band exposure of the NGC 1399 field with the NTT, which Gauthier Mathys kindly obtained for us. We used about 40 stars in the field to derive the coordinate transformation between the CTIO and NTT images, using the IRAF processing software. (First it was necessary to filter out the effects of the steep luminosity gradient of the underlying elliptical galaxy.) The coordinate transformation over this small field turned out to be highly nonlinear: for adequate accuracy, a 3rd degree chebyshev function with cross terms was needed.

Our next problem was that the software allowed us to apply the coordinate transformation only to images: we were unable to find a way (short of writing our own programme) to obtain the NTT (x,y) coordinates directly from our CTIO (x,y) coordinate table. One quick and accurate way around this problem was to generate an artificial CTIO image with fake stars at the PNe (x,y) pixel positions. We applied the CTIO → NTT coordinate transformation to this artificial image and then derived the PNe (x,y) positions in the NTT-fp using a centring algorithm. Finally we used the ascii file with these (x,y) positions to produce the MOS masks.

The CTIO image of NGC 1399 covered an 8′ × 8′ field with PNe present over this entire area. The punch area for the MOS masks is 5′ × 8′, so two MOS masks were needed to include all the known PNe of NGC 1399. One mask was offset 75″ East of the nucleus of NGC 1399, and the other 75″ West, with an overlap of 2.4′ × 8′. Our ascii file with the PN coordinates was adjusted accordingly: we decided which PNe went to which plate, and an offset to their x-coordinates was applied depending on whether they would appear on the East or West plate. The updated MIDAS tables corresponding to the East and West masks were copied to ∗.msk files, from which the MOS plates were punched. In addition to the slitlets punched at the PNe positions, two slitlets were punched in each MOS mask at positions correspondent to reference stars in the NGC 1399 field which we used to monitor the telescope pointing. The East mask contained 40 slitlets corresponding to 38 PNe plus the two stars, and the West mask has 42 slitlets (40 PNe and the two stars). In the overlapping region between the two masks there are 21 PNe and the two reference stars.

Before each exposure, we took an image at the mask position and then used the MIDAS task "pointing" to evaluate the x,y shifts needed to put the reference stars back at the centres of their punched slits. PNe spectra were taken only after our pointing had been checked: we noticed that the process of making calibration lamp exposures caused a significant shift of the telescope position, so a check for pointing was essential after each calibration.

The Observations. – Spectra were taken for the East field on November 14, with an average seeing FWHM = 0.9″ and a total integration time of 3.8 hrs. The spectra for the West field were acquired on November 16, with an average seeing of FWHM = 1.0″ and a total integration time of 4.7 hrs. One night was lost due to bad weather. The success of the observations depended very much on having the best possible image quality, so we performed imaging analysis twice a night and regularly checked the focus.

3. Data Reduction

Flat field exposures for the two MOS plates were taken with the internal lamp, the grism and the interference filter. The bias frames were flat and constant throughout each night, and so were the dark frames. Unfortunately, the performance of the Loral CCD was compromised by charge trapping problems which could not be corrected: some PNe were lost in the dark columns which extended for some tens of pixels.

Before combining all the frames obtained during one night, we carefully checked for any shifts in x and y which could possibly effect our velocity measurements. The stability of EMMI is exceptional. The average shift in the x (wavelength) direction was $\Delta x = 0.08$ pixels, which corresponds to a negligible velocity error of $\Delta v \cong 8$ km/s. The shifts in the y-direction were also very

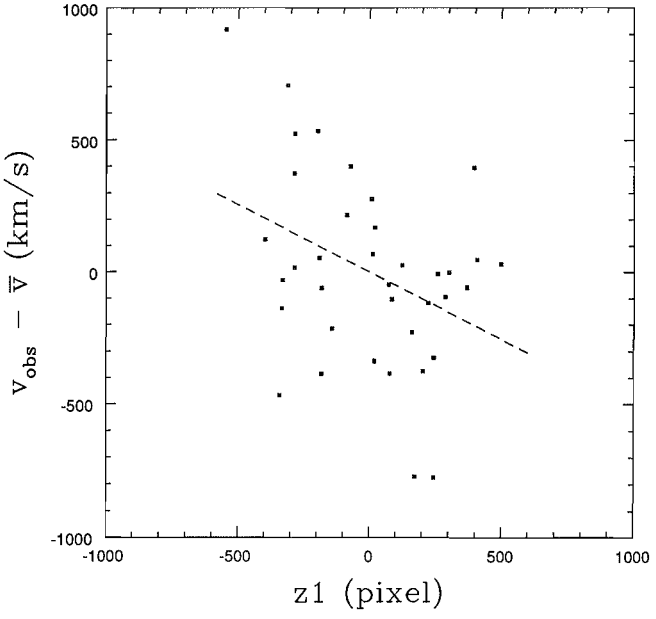

Figure 3: $v_{obs} - \bar{v}$ *vs. z1, where z1 is the linear coordinate along the direction z1 of strongest velocity gradient. One pixel is 0.47 arcsec. The rotation is evident. The dashed line indicates the linear fit to the data.*

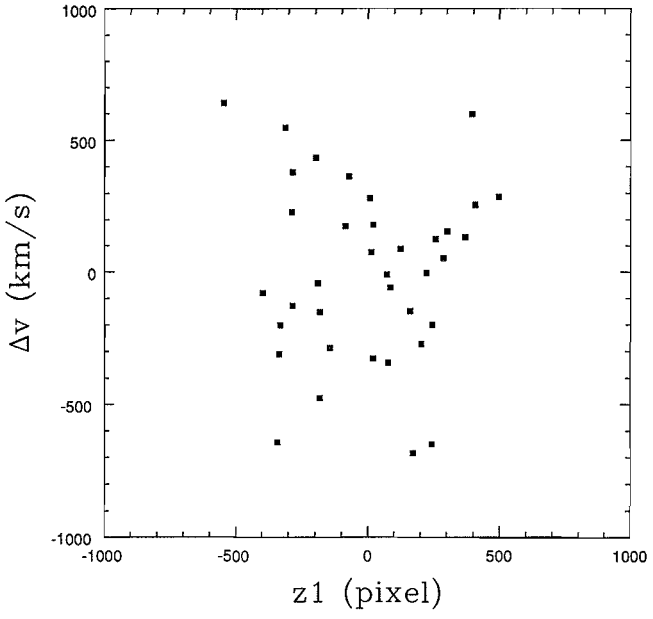

Figure 4: *The velocity residual about the linear rotation fit Δv vs. z1, where* $\Delta v = v_{obs} - v_{rot}$ and z1 is the linear coordinate along the direction of strongest velocity gradient. One pixel is 0.47 arcsec. The velocity residuals obtained after the subtraction of the rotation component are scattered around (0,0), and their distribution appears symmetric.

small, less that $\Delta y = 0.19$ pixels on both nights.

Therefore, we could directly combine the MOS frames and the calibration exposures obtained during a single night; after combining, the two resulting MOS frames appeared free of cosmic rays. Then the 2D spectra of each PN were extracted and wavelength calibrated using the corresponding He-Ar spectrum in the combined arc calibration frames. Figure 1 shows examples of these 2D spectra.

At this point we looked for the [OIII] emission from the PN in the expected wavelength range[1] and at the expected PN y-position along the slitlet. We then subtracted the sky background, using the average of the sky rows for each individual spectrum. The rows where the [OIII] emission appears were averaged and the redshifted λ5007 Å measured using a Gaussian fit.

Spectra were extracted for 54 PNe, and we were able to measure velocities for 37 PNe. Of the 21 PNe which appeared on both the East and the West MOS frames, 14 have velocity measurements, and they give us a direct estimate of the velocity errors. The distribution of their $\delta v = v_{East} - v_{West}$ gives $v_{mean} \cong -15$ km/s, indicating that there is no systematic velocity shift between the two nights, and a $\sigma(\delta v) = 103$ km/s which gives an error of ± 72 km/s for a single velocity measurement.

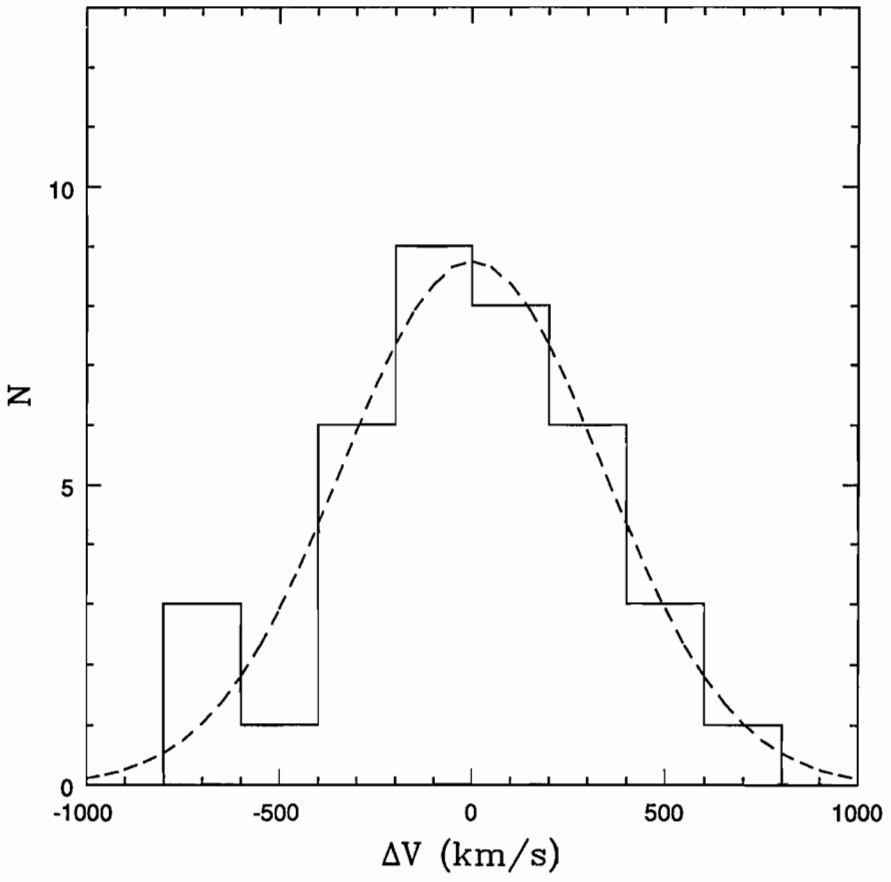

Figure 5: *Histogram of Δv in bins of 200 km/s. The distribution is well approximated by a Gaussian (dashed line) with $\Delta v_{means} = 0$ km /s and $\sigma = 342$ km/s. No systematic residuals are left after the subtraction of the rotation velocity component.*

4. Results

With the NTT and the EMMI/MOS facility, we have been able to measure velocities for PNe in the outer parts of the cD galaxy NGC 1399, between 5 and 24 kpc from the centre. This interesting region lies outside the limits of the integrated light observations, but overlaps the region covered by the globular cluster observations of Grillmair et al. (1994).

The PN velocities show that the outer parts of NGC 1399 are rotating. A 2D linear fit to the data gives a mean velocity $\bar{v} = 1503$ km/s and a maximum velocity gradient of (1.09 ± 0.46) km/s per arcsec along P.A. = –35° ± 26°. This maximum velocity gradient corresponds to ± 290 km/s over ± 24 kpc. The rotation can be seen in Figure 2, which shows the PN positions in the NGC 1399 field indicated with open circles if their velocities are below $\bar{v}$, and with full circles if their velocities are above $\bar{v}$; the size is proportional to the ratio $|v_{obs}/\bar{v} - 1|$. Figure 3 shows the observed velocity against the linear coordinate z1 along the direction of maximum gradient; again, the rotation is evident. The detailed pattern of rotation (now shown here) is more nearly cylindrical than spheroidal.

Figure 4 shows the distribution of residual velocities $\Delta v = v_{obs} - v_{rot}$ against z1. There is no residual velocity gradient, and the σ of the residual velocities is $\sigma_{\Delta v} = 342$ km/s. The histogram of Δv values shown in Figure 5 is well represented by a Gaussian distribution with $\Delta v_{mean} = 0$ and $\sigma_{\Delta v} = 342$ km/s. (The velocity dispersion of the raw observed velocities is $\sigma(v) = 364$ km/s.)

Figure 6 shows the radial distribution of Δv. It appears that the velocity distribution of the PNe is not isothermal: the scatter of Δv increases with radius. If we divide our data into two subsamples with $r < \bar{r}$ and $r > \bar{r}$, where $\bar{r} = 2.6'$ is the average radius of the PN sample, we obtain $\bar{r}_1 = 1.9'$ and $\sigma_1 = 269$ km/s for the inner subset, and $\bar{r}_2 = 3.4'$ and $\sigma_2 = 405$ km/s for the outer subset, indicating that the velocity dispersion of the stellar component in NGC 1399 increases with radius. In Figure 7 we put together the measurements of velocity dispersion from integrated light and globular clusters (from Grillmair et al. 1994) and our two PN points (r_1, σ_1), (r_2, σ_2) in the σ – log r diagram for NGC 1399. The error bars show the measuring errors of the velocity dispersions for the integrated light data and the statistical errors for the velocity dispersion of the PNe and globular clusters. The PN velocity dispersion points fall nicely in the region between the globular clusters and the integrated light. They confirm previous indications (Grillmair et al. 1994) that the velocity dispersion increases in the outer parts of NGC 1399, giving a value for $M/L_B(4')$ greater than 80. For comparison, the dotted line in Figure 7 shows our linear (i.e. solid body) fit to the rotation of the PN system. We note that, as in Cen A, the outer stellar halo of NGC 1399 shows significant rotation, while its globular cluster system is apparently not rotating.

5. Conclusions

At present the NTT with EMMI is the only system in the world with which we can acquire spectra of distant extragalactic PNe with [OIII] λ5007 Å fluxes below about $3 \cdot 10^{-17}$ ergs $cm^{-2} s^{-1}$. We have used this system in multislit mode

[1] The expected wavelength range is 5031 ± 17Å, corresponding to the galaxy redshift of 1440 km/s (RC3) ± 1000 km/s.

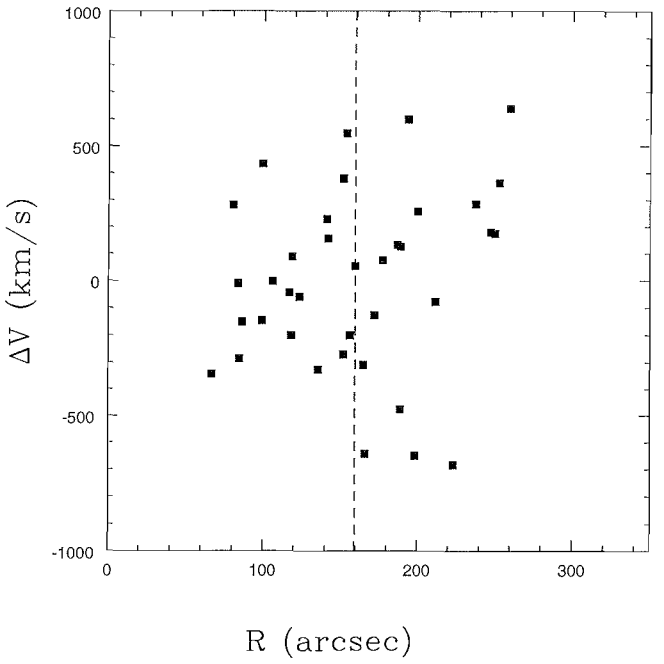

Figure 6: *Δv vs. radius r: the residual velocity data appear to be more scattered at larger radii. The dashed line indicates the average radius of the distribution, at $\bar{r}$ = 2.65 arcmin.*

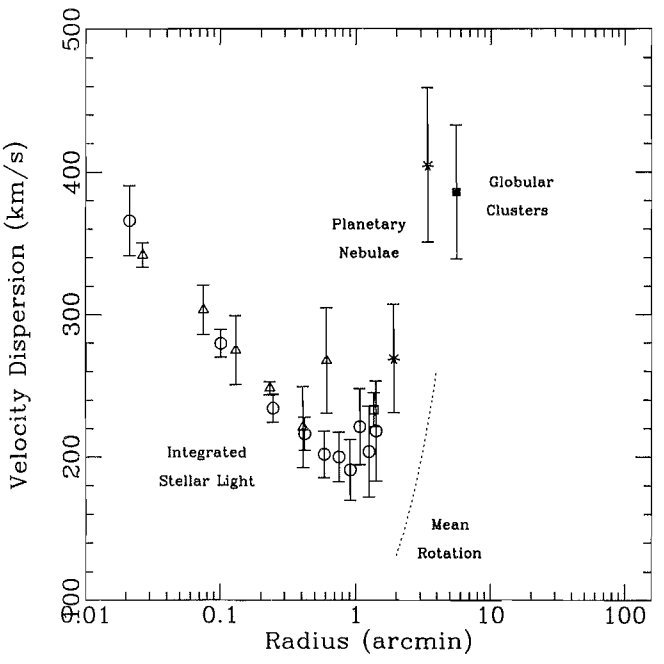

Figure 7: *Velocity dispersion σ vs log r for (i) integrated light of NGC 1399 (open circles and triangles), (ii) the globular clusters in NGC 1399 (filled square) and (iii) our PNe velocity measurements (stars). The dotted curve shows the rotational velocity for our solid body rotation fit to the velocities of the PNe. For comparison, the surface brightness of NGC 1399 at a radius of 3 arcmin is μ_B = 24.5 mag arcsec^{-2}.*

to measure radial velocities of a sample of PNe in the outer regions of NGC 1399. From the PNe, the outer parts of this giant elliptical show substantial rotation. However, the velocity distribution of the globular clusters around NGC 1399 from Grillmair et al. (1994) shows no significant evidence of rotation. So it seems that the stellar halo of NGC 1399 rotates rapidly and its globular cluster system is not rotating at all (cf. Centaurus A).

The direction of maximum velocity gradient among the PNe in NGC 1399 lies in P.A. = –35°, which is close to the direction of the nearby giant elliptical NGC 1404. It is possible that the rotation of the old stars (PNe) in the outer parts of NGC 1399 could be induced by tidal interaction between the two giant ellipticals. The absence of rotation in the globular cluster system might then suggest that the very extended old stellar population in this cD galaxy, including the PNe, is part of the tidal debris, while the globular clusters belong to the original NGC 1399.

More generally, if the rapid rotation of the PN system of NGC 1399 reflects the mean motion of the bulk of the luminous component in the outer regions of this galaxy, then the outer regions contain a large amount of angular momentum. We can show that the total specific angular momentum J/M of this giant elliptical is in fact comparable with that of giant spirals. However, we know that for the inner parts of giant ellipticals (including NGC 1399) the J/M is typically an order of magnitude lower than for spirals of comparable mass (Fall 1983). What is predicted by theoretical studies of galaxy formation? Zurek et al. (1988) and Quinn & Zurek (1988) have studied the J/M distribution for dark halos as the halos are built up by secondary infall in their cosmological simulations. Redistribution of energy and angular momentum occurs through the interaction of the clumps in the aggregating system. Clumps with lower J/M become more bound and lose J/M as they settle to the centre of the system, while the less bound objects with higher J/M gain angular momentum and form the outer parts of the resulting system. This secondary infall picture produces a system with low J/M in the inner regions and higher J/M in the outer regions. Although these models represent aggregating dark halos, the gross dynamical properties (the λ-parameter, shape distribution, mean motion v/σ) of these theoretical dark halos and the luminous components of real elliptical galaxies are very similar, and we can regard our observations of the outer parts of NGC 1399 as consistent with these secondary infall models.

Our velocity dispersion measurements for the PN confirm the previous evidence from the globular cluster kinematics for a high dark matter content in NGC 1399, and are consistent with a M/L_B ratio at least 80 within 4 arcmin.

Acknowledgements

We are grateful to S. D'Odorico, J. Melnick, G. Mathys, and the NTT night staff for much assistance before and during our run at the NTT, to P. Quinn for advice on galaxy formation, and to M. Bessell and G. Bloxham for their help with acquisition of the filter. The assistance of P. Le Saux, in modifying the EMMI punch programme and preparing the MOS masks by the non-standard process described above, was essential to the success of this observing run and is gratefully acknowledged.

References

Capaccioli, M., & Longo, G. 1994. Preprint.

Fall, S.M.F. 1983. In *IAU Symposium 100, Internal Kinematics and Dynamics of Galaxies*, ed. E. Athanassoula (Dordrecht: Reidel), p. 391.

Grillmair, C.J. et al. 1994. *ApJ* **422**, L9.

Harris, H.C., Harris G.L.H., Hesser, J.H. 1988. In *IAU Symposium 126, The Harlow-Shapley Symposium on Globular Cluster Systems in Galaxies*, eds. J.E. Grindlay and A.G. Davis Philip (Dordrecht: Reidel), p. 205.

Hui, X., Ford, H.C., Freeman, K.C., Dopita, M.A. 1993. Preprint.

McMillan, R., Ciardullo, R., Jacoby, G.H. 1993. *ApJ* **416**, 62.

Quinn, P.J. & Zurek, W.H. 1988.*ApJ* **331**, 1.

Zurek, W.H., Quinn, P.J., Salmon, J.K. 1988. *ApJ*, **330**, 519.